II International Conference on Particle-based Methods - Fundamentals and Applications
PARTICLES 2011
E. Oñate and D.R.J. Owen (Eds)

# NUMERICAL STRESS PROBING ON A 2D MODEL GRANULAR MATERIAL

**F. FROIIO*, J.-N. ROUX†**

* Laboratoire de Tribologie et Dynamique des Systèmes
Ecole Centrale de Lyon, 36 av. Guy de Collongue
69134 Ecully cedex, France
e-mail: francesco.froiio@ec-lyon.fr, ltds.ec-lyon.fr

†Laboratoire Navier
Université Paris-Est, 2 Allée Kepler, Cité Descartes
77420 Champs-sur-Marne, France e-mail: jean-noel.roux@lcpc.fr, www.lcpc.fr

**Key words:** Granular Materials, DEM, Stress probing, Elastoplasticity

**Abstract.** We use DEM simulations on a simple 2D model of a granular material to measure its deformation response to small stress increments of arbitrary directions (stress probes) and assess the applicability of the classical concepts of elastoplasticity. We impose stress increments in the space of principal stresses components, to numerical specimens selected at various intermediate states along the biaxial compression path. The elastic part of the incremental response is systematically identified by building the elastic stiffness matrix of well-equilibrated configurations. Plastic strain increments are computed standing on the partition hypothesis for strain increments into elastic- and plastic parts. The domain of validity of the partition hypothesis is discussed, playing extensively with the magnitude of the stress increments, in order to identify a range in which the incremental response is homogeneous of degree 1 and the essential features of plasticity models can be observed. We investigate in particular the existence of a plastic flow rule with a clearly defined plastic flow direction and yield criterion. The robustness of these features is tested over a range of contact stiffness levels and against the dominant deformation modes (*i.e.*, based on contact deformation or network rearrangement).

## 1 Introduction

Elastoplastic models for granular materials under quasistatic loading conditions were first developed by adapting the key features of metal plasticity models to the frictional-cohesive nature of soils, on a large basis of phenomenological observation in laboratory testing [1, 2]. The continuously improving performances of discrete numerical simulation tools offer nowadays the possibility to run reliable testing campaigns on "virtual" granular

specimens. In complement to physical testing, discrete numerical simulations provide flexibility, repeatability and an open window on the microscopic processes driving the phenomenologically observable behaviour. This paper summarizes some recent advances of an ongoing work that should be ascribed in the relatively small number of studies where the essential features of elastoplastic models for granular materials are investigated by a systematic use of a numerical implementation of the *stress probing technique* [3, 4, 5], as first addressed by Bardet [6, 7] since 1989. The simple idea of this technique is to measure the deformation response of "identical" specimens to a rose of supposedly-infinitesimal stress increments (stress probes) in a comprehensive spectrum of stress directions. Clearly, a prerequisite for this technique is the capability to obtain as many identical specimens as the number of stress increment directions under considerations. This facts makes its application prohibitive, therefore rare, in physical testing [8], while it entails no major difficulty in numerical testing.

Among the classical features of elastoplasticity that have been investigated by previous researchers applying the stress probing technique to granular materials, one can mention (i) the character of *rate-independence* of the material response, (ii) the *partition hypothesis* for the deformation increments into elastic- and plastic components and (iii) the existence of a *plastic flow rule* with clearly identified *plastic flow direction* and *yield criterion*. In this study, those features are reconsidered in an enlarged and unified context, by varying a small number of material- and texture parameters. In addition, we pay particular attention to (iv) the identification of an appropriate range of *stress increment amplitudes* for the measurements to be actually expressive of the incremental (tangent, infinitesimal) response. We show why this apparently technical aspect can affect the measurement results substantially. We limit ourselves, in this paper, to some results concerning stress probes under biaxial conditions. For some anticipations on the extension of the method to the incremental response under rotation of principal stress axes, we refer the interested reader to a preliminary study in Ref. [9].

In the following sections we introduce briefly the numerical procedure of specimen preparation and the inherent parameters. Next, we address some results concerning the issues at points (i)-(iv) in the above list and conclude with a short summary.

## 2 Specimen preparation and investigation points

The numerical samples tested in this work are disk assemblies of 5600 particles, with diameters uniformly distributed in the range $[0.7d, 1.3d]$ about the average diameter $d$. Two contacting particles interact by a unilateral normal contact force $F_N$ and a tangential contact force $F_T$. The simple rheological model for the normal contact force consists of an elastic- plus a viscous contribution as functions of the contact deflection $h_N \geq 0$ and its time rate, respectively:

$$F_N = K_N h_N + \alpha_N \dot{h}_N \, .$$

The tangential contact force is computed as the elastic response to the relative contact sliding $h_T$ and is bounded by Coulomb-friction, i.e.,

$$F_T = K_T h_T \,, \quad F_T \leq \mu F_N \,,$$

where $\mu$ is the contact-friction coefficient. We neglect any volume actions but inertial ones.

At the virgin state, the disk assembly fills a rectangular cell, approximately square, aligned along directions 1 (lateral) and 2 (axial). The cell can undergo generic affine deformations in order to accommodate the most general deformation of a granular REV under small strains. Bi-periodic boundary conditions are implemented according to the Parrinello-Rahman and Lees-Edwards techniques for molecular dynamics [10, 11]. The components of the Cauchy stress tensor $\boldsymbol{\sigma}$ can be retrieved at any time either from inter-particle forces inside the REV, via the classical Love formula, or by simple averages on inter-particles forces across the cell boundaries. Quasi-static conditions being ensured in our tests, the two procedures provide sensitively the same measurements. The components of the infinitesimal strain tensor $\boldsymbol{\epsilon}$ are obtained by a direct quantification of the affine deformation of the bounding periodic cell. The loading history of the generic specimens to be tested against stress probes consists of a standard biaxial compression procedure, with a first stress-rate-controlled isotropic compression and a subsequent axial compression at constant axial strain-rate and constant value $P$ of the lateral pressure $\sigma_{11}$.

The biaxial tests executed for this study can be classified with respect to a small comprehensive number of non-dimensional parameters taking into account material properties and test conditions: (i) the stiffness parameter $\kappa = K_N/P$, setting the scale of contact deflections; (ii) the contact friction coefficient $\mu$; (iii) the damping parameter $\zeta = \alpha_N/\sqrt{2K_N m}$ (with $m$ the mass of the typical particle of diameter $d$) discriminating the underdumped- from the overdamped regime of an elementary oscillator connecting two particle of mass $m$ by a spring of constant $K_N$; (iv) the inertia parameter $\gamma = \dot{\epsilon}_{22}\sqrt{m/P}$, setting the scale of inertia forces. In our study we set $K_T$=$K_N$ and fix $\mu = 0.3$ for sake of simplicity. We choose $\zeta = 0.9$ in order to keep particle interactions slightly overdumped and so accelerate the numerical convergence. The inertia parameter $\gamma$ is bound to $10^{-4}$, to ensure quasistatic conditions of testing. Finally, the stiffness parameter $\kappa$ takes the values $10^3$, $10^4$ and $10^5$. This first set of parameters controlling the condition of biaxial testing can be extended by introducing the stress ratio $\varsigma = Q/P$, where $Q$ is the value of axial pressure $\sigma_{22}$ at which the specimen is tested against stress probes. This extended set of parameter controls the conditions of stress probing. In the large majority of the tests considered here, the stress probes were applied at the *investigation points* $\varsigma = 1.2$, 1.4, 1.6 and 1.8.

A numerical refinement of the isotropic consolidation procedure (prior to axial loading in biaxial tests) allows to obtain "twin" specimens that are macroscopically undistinguishable, namely in terms of stress $\boldsymbol{\sigma}$ and solid fraction $\Phi$, but differ in terms of texture [12, 13, 14]. As shown in Table 1, we apply here this procedure in order to im-

Table 1: Biaxial test families and values of variable parameters.

| Family | $\kappa$ | $\varsigma$ (*ca.*) |
|---|---|---|
| A3 | $10^3$ | $1.2, 1.4, 1.6, 1.8$ |
| A4 | $10^4$ | $1.2, 1.4, 1.6, 1.8$ |
| A5 | $10^5$ | $1.8, 1.9$ |
| B3 | $10^3$ | $1.2, 1.4, 1.6, 1.8$ |
| B4 | $10^4$ | $1.2, 1.4, 1.6, 1.8$ |
| B5 | $10^5$ | $1.2, 1.4, 1.6, 1.8$ |

prove the variety of the population of our specimens. Biaxial tests of type A4 and B4, for example, share the same stiffness parameter $\kappa = 10^4$, but the tests in the first family were "numerically lubricated" during the isotropic consolidation by temporarily dimming $\mu = 0$, which lead to much larger, almost maximal, values of the coordination number $z$ (about 4, *vs.* 3 *ca.* for a specimen of type B4). The same difference can be acknowledged between tests of the type A3 and B3 (both for $\kappa = 10^3$) or A5 and B5 ($\kappa = 10^5$, resp.). Typical axial loading curves are shown in Fig 1 for biaxial tests of type A3, A4 and A5. At small strains, comparing different curves at equal stress ratio $\varsigma$, the axial strain scales with $\kappa^{-1}$, indicating that the contact deformation drives the macroscopic response [12]. Fig 2 refers to axial compression in biaxial tests of type B3, B4 and B5. The inherent microscopic mechanism of deformation at small strains is now the continuous network rearrangement by microscopic instabilities, which makes the macroscopic behaviour actually independent from the contact deformations and therefore almost insensitive to the stiffness parameter $\kappa$: the loading curves superposes at small strains.

## 3 Incremental response under biaxial loading conditions

The values of stress ratio in Table 1 indicate the investigation points for the stress probing procedure, depending on the biaxial test family. At least two specimens from each family were submitted to parallel tests, in order to assess the degree of repeatability, which was found satisfactory. The stress probes were applied along sixteen different directions, uniformly distributed in the plane of principal stresses (from "0A" to "0P"in Fig. 3). Along each stress direction we applied twelve stress increment levels, corresponding to as many multiples of $2\sqrt{2}\,P \times 10^{-3}$. The anelastic (supposedly-plastic) strain increments $\delta\boldsymbol{\epsilon}^P$ were obtained by computing the difference

$$\delta\boldsymbol{\epsilon}^P = \delta\boldsymbol{\epsilon} - \delta\boldsymbol{\epsilon}^E \tag{1}$$

between the total strain increments $\delta\boldsymbol{\epsilon}$ and the elastic strain increments $\delta\boldsymbol{\epsilon}^E$. The validity of the partition hypothesis (Eq. 1) is checked here *a posteriori*, by giving evidence of a plastic flow rule and a yield criterion, as detailed in the following paragraphs where we will be focusing on results from stress probing on specimen issued from biaxial tests of

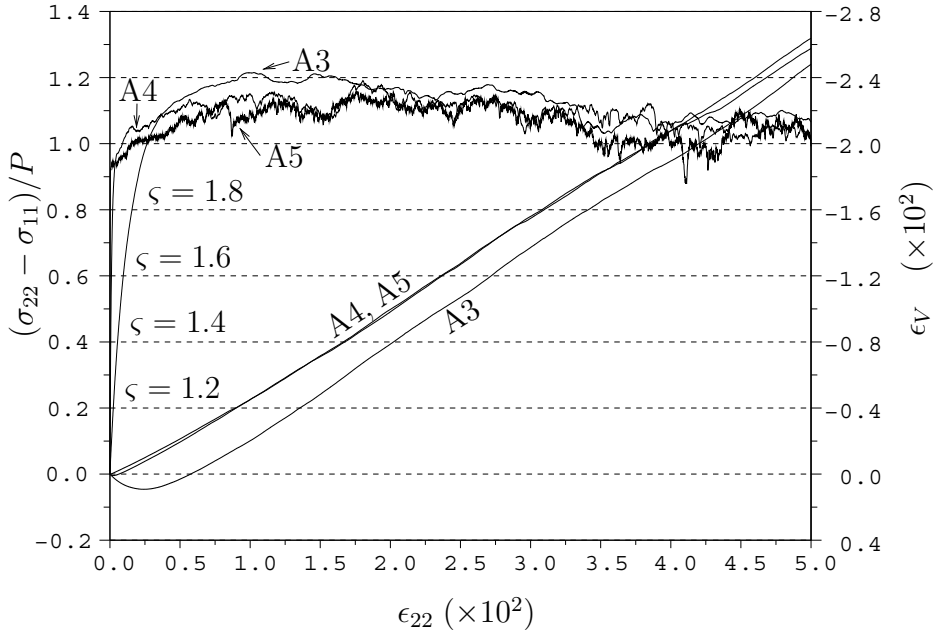


Figure 1: Normalised deviatoric stress *vs.* axial strain and volumetric strain *vs.* axial strain for typical biaxial tests of type A3, A4 and A5.

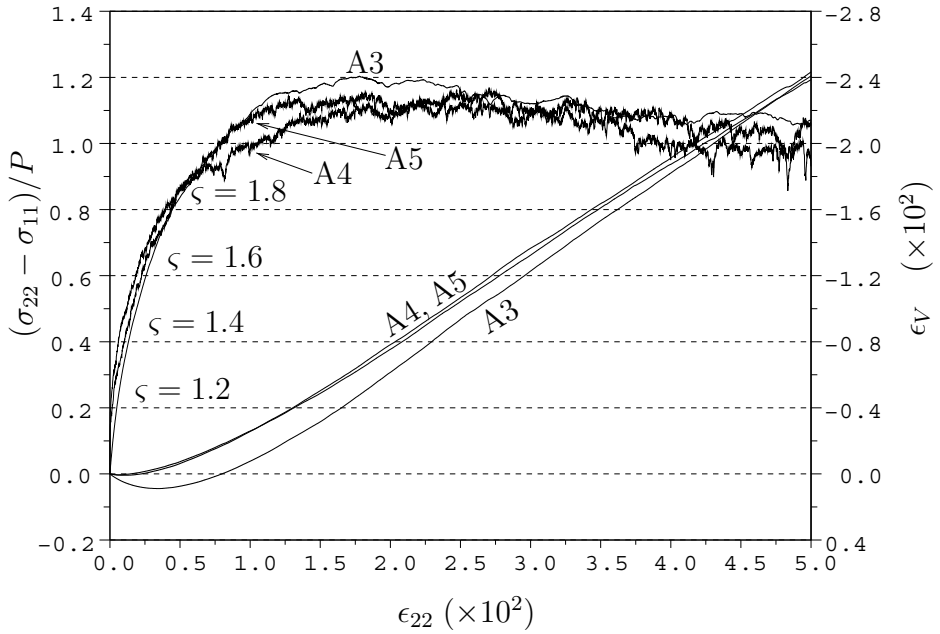


Figure 2: Normalised deviatoric stress *vs.* axial strain and volumetric strain *vs.* axial strain for typical biaxial tests of type B3, B4 and B5.

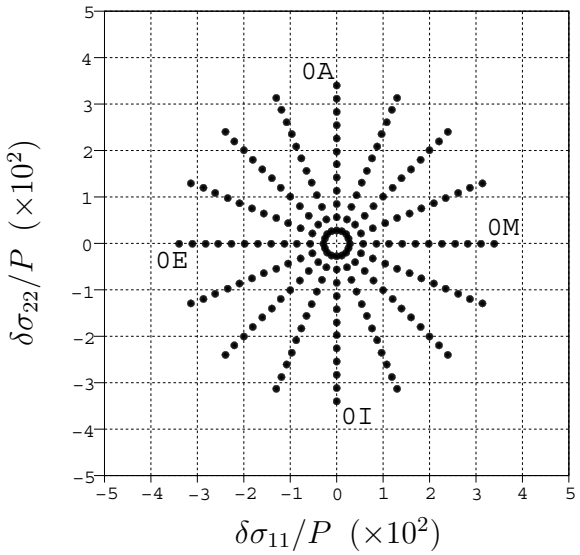


Figure 3: Rose of normalised stress increments.

type A4 and B4. We will finally point out the main differences with respect to other families of specimens, when relevant.

The elastic strain increments cannot be observed directly and were systematically computed according to the assigned stress increments *via* an elasticity tensor built by assembling the contribution of the contact stiffnesses across the contact network [14]. As an example, in Fig. 4 we represent the incremental elastic response of a specimen of type A4 to the stress probes in Fig. 3, applied at the investigation points $\varsigma = 1.2$ and $\varsigma = 1.8$. The specimen exhibits a marked elastic anisotropy, slightly evolving during the axial loading.

For the same specimen and investigation points, Fig. 5 shows the plastic strain increments $\delta\boldsymbol{\epsilon}^P$ computed according to Eq. 1 and compared to the elastic strain increments. The plastic strain increments align neatly along a plastic flow direction in the plane of principal strains. The inclination of such direction with respect to the $\epsilon_{11}$ axis ranges from 132° (for $\varsigma = 1.2$) to 138° (for $\varsigma = 1.8$, resp.). A plastic flow direction is clearly identified also for specimens from biaxial tests in the family B4, as shown in in Fig 6 for the investigation point $\varsigma = 1.8$. The inherent plastic flow direction, measured by an angle of 142° with respect to the $\epsilon_{11}$ axis, is approximately the same as the homologue case in Fig. 5, but the plastic strain increments are about one order of magnitude larger. The elastic contribution appears now negligible in comparison. It is interesting to remark how the plastic strain increments in Fig. 5 group in segments along the plastic flow direction, consistently with the leading deformation mechanism for this type of specimens, by alternate instabilities and rearrangement of the contact network (*cf.* Sec. 2).

Qualitatively-similar features or the same features where observed for all tested specimens: (i) a clear plastic flow direction can always be identified; (ii) compared to plastic

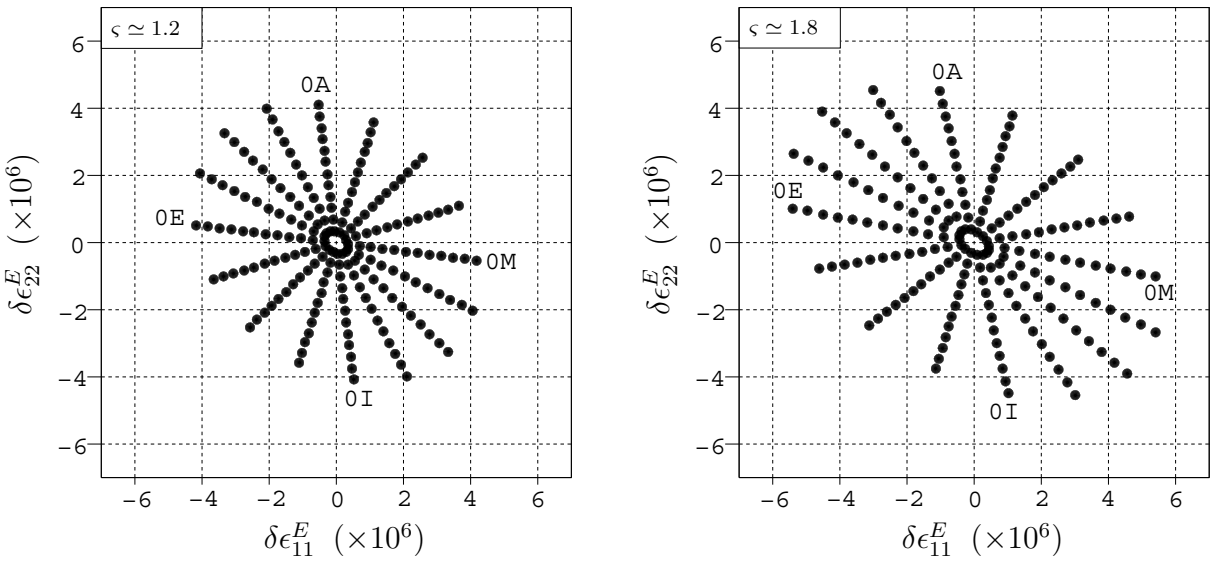


Figure 4: Elastic response for a specimen at stress ratio $\varsigma \simeq 1.2$ (left) and $\varsigma \simeq 1.8$ (right) from a biaxial test of family A4.

strain increments, the contribution of the elastic increments tends to reduce with increasing values of the stress ratio and of the stiffness parameter; (iii) such contribution is much weaker, in some cases negligible, for low-coordination specimens (*i.e.*, from families B3, B4 and B5).

We now consider the flow rule

$$\delta\boldsymbol{\epsilon}^P = \begin{cases} \frac{1}{E^P}(\delta\boldsymbol{\sigma}\cdot\boldsymbol{\xi})\,\boldsymbol{\pi} & \text{if} \quad f(\boldsymbol{\sigma})=0 \quad \text{and} \quad \delta\boldsymbol{\sigma}\cdot\boldsymbol{\xi}\geq 0 \\ 0 & \text{if} \quad f(\boldsymbol{\sigma})=0 \quad \text{and} \quad \delta\boldsymbol{\sigma}\cdot\boldsymbol{\xi}<0 \\ 0 & \text{if} \quad f(\boldsymbol{\sigma})<0 \end{cases} , \tag{2}$$

where the second-order tensor $\boldsymbol{\pi}$ ( $\|\boldsymbol{\pi}\|=1$ ) represents the plastic flow direction discussed previously, $E^P$ is the plastic stiffness modulus and the second-order tensor $\boldsymbol{\xi}$ ( $\|\boldsymbol{\xi}\|=1$ ) identifies the outward-oriented normal to the yield locus seen here as an hyper-surface in the associated stress space. It is worth recalling that these three quantities should not depend on the applied stress increment, but only on the actual state variables. The directional issue, *i.e.* that of the existence of a plastic flow direction $\boldsymbol{\pi}$, has just been settled and in order to validate the flow rule one just needs to exhibit a satisfactory fitting of the numerical data with Eq. 2 in norm. A plot of this type is shown in Fig. 7 for the four investigation points of a biaxial test in the family A4. The norm $\|\delta\boldsymbol{\epsilon}^P\|$ of the plastic strain increments is plotted against the component of the respective stress increments $\delta\boldsymbol{\sigma}$ along $\boldsymbol{\xi}$. The plot takes into account only positively-oriented stress increments (*i.e.*, such that $\delta\boldsymbol{\sigma}\cdot\boldsymbol{\xi}\geq 0$) and all the stress increment amplitudes are represented, undistinguished. Following Eq. 2, for small-enough stress increments, the four curves should conform to as

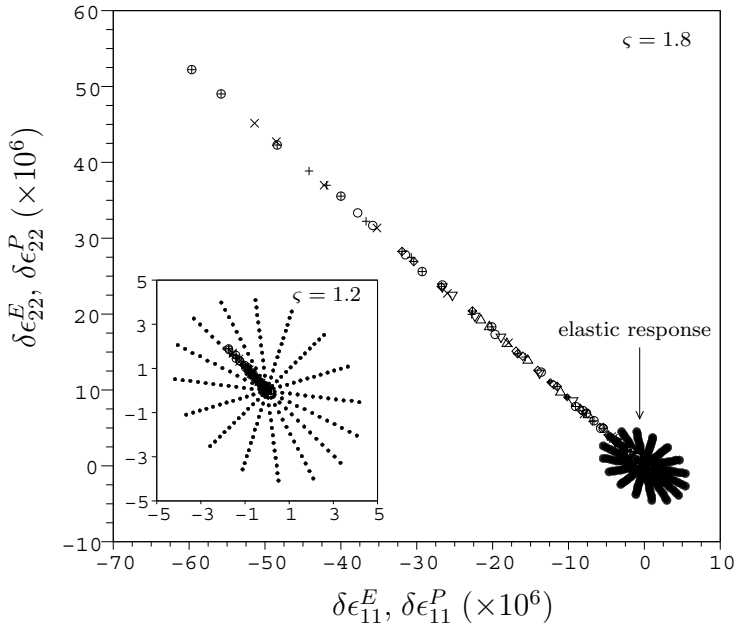


Figure 5: Elastic vs. plastic response of a specimen at stress ratio $\varsigma = 1.2$ (inner frame) and $\varsigma = 1.8$ (outer, resp.) from a biaxial test of family A4.

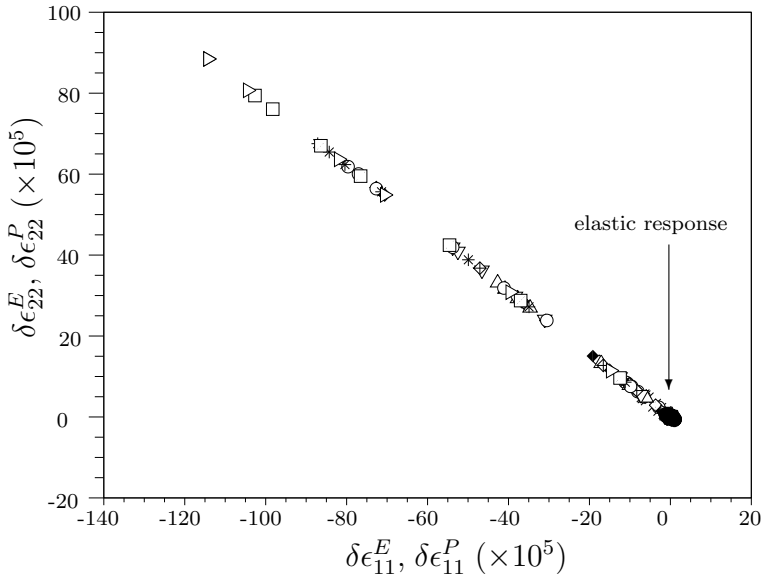


Figure 6: Elastic vs. plastic response for a specimen at stress ratio $\varsigma = 1.8$ from a biaxial test of family B4.

many straight lines passing by the origin of the plot. In practical terms, the appropriate size of the stress increments should note exceed the range put in evidence by the frame in the figure, out of which the measurements deviate substantially from a linear relation. The suggested range corresponds roughly to the eighth level of stress increment amplitudes in Fig. 3. According to the results obtained insofar from specimens of type A3, A4 and A5, this range seems also to depend sensitively on stiffness parameter $\kappa$: the higher its value the smaller the maximal allowed relative amplitude $\|\delta\boldsymbol{\sigma}\|/P$ of the stress increments for an efficient fitting of the flow rule.

On the other hand, the stress increments cannot be chosen arbitrarily small. A first technical but obvious reason is that they cannot be assigned at the scale set by the accuracy of the numerical algorithm. A second reason appears from Fig. 7, in which the dashed line interpreting the plot for $\varsigma = 1.8$ gives evidence of a slight offset from the origin. This feature, appearing systematically for this type of specimens, might be interpreted as a parasite effect of the specimen preparation procedure. After the investigation point was reached during the axial compression, the numerical simulation was continued, at constant stress, for the time needed to reach a finely-equilibrated configuration, in order not let dynamical effects interfere with the response to stress probes. The observed offset might therefore be seen as a restored minimal elastic region, close to the origin of the plot, due to a slight unavoidable rearrangement of the contact network and consequent loss of plastic memory during the "creep" transition before stress probing.

The values measured on the horizontal axis in Fig. 7 depends on the choice of the quantity $\boldsymbol{\xi}$, *i.e.*, of the outward-orient normal to the yield locus. The direction $\boldsymbol{\xi}$ of the stress space selects the component of the stress increment that is retained as "active" by the flow rule. Arbitrary choices of $\boldsymbol{\xi}$ produce extremely scattered plots, and meaningful curves can only be obtained when $\boldsymbol{\xi}$ points at a precise direction of the stress space. The existence of this particular direction is an implicit, final confirmation of the validity of the flow rule in Eq. 2. Moreover, the minimisation of the plot scattering proves also to be a robust procedure for the detection of the normal to the yield locus. We refer the interested reader to Ref. [9] for systematic measurements of $\boldsymbol{\xi}$ quantity and the plastic flow direction $\boldsymbol{\pi}$ in the whole range of parameters and specimen families considered in this work. We anticipate that those masurement confirm the non-associative character of the flow rule, which is a classical result in granular plasticity. We finally remark that the same qualitative observation concerns the specimen from biaxial tests of type A3 and A5.

The case of a specimen from biaxial tests of type B4 is represented in Fig. 8, where the main differences with respect to the case A4 can be found by looking at the plot for the investigation point $\varsigma = 1.8$. The latter can be observed in more detail as it sets the scale of the vertical axis. The staircase shape of the plot is consistent with the leading deformation mechanisms for specimens from biaxial tests in the families B3, B4 and B5, that deform by repeated instabilities and rearrangements of the contact network. This observation is in accordance with the analogous remark on Fig. 6. Practically speaking, in

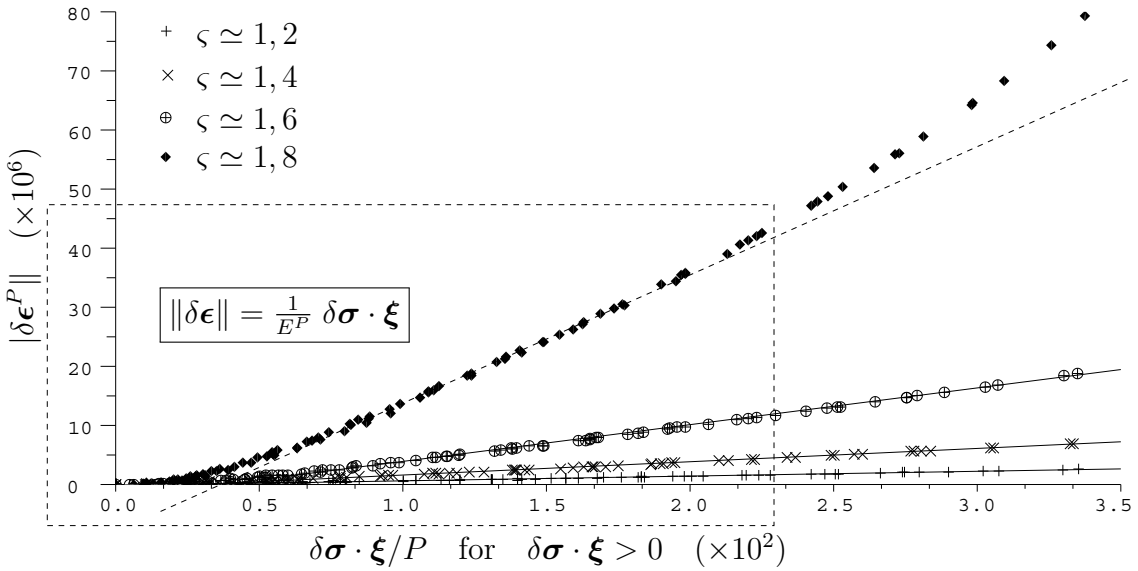


Figure 7: Plastic strain increment amplitude *vs.* active part of the stress increments for specimens at stress ratios $\varsigma \simeq 1.2$ to 1.8 from a biaxial test of family A4. Stress increment amplitudes as mutliples of $2\sqrt{2}\,P \times 10^{-3}$.

order to get meaningful measurements of the plastic stiffness modulus $E^P$ for specimens of this type, one needs to set the order of magnitude of the stress increments at a larger scale, at which the segmentation of the plot is averaged out. The result of this rescaling is suggested in Fig. 9 which results from the application of stress increments of four different amplitudes, for as many multiples of $2\sqrt{2}\,P \times 10^{-2}$, roughly one order of magnitude higher than those in Figs. 7 or 8.

## 4 Conclusions

We have presented a robust numerical method, via DEM simulations, for the measurement of the incremental response of model (2D) granular materials. The numerical implementation of this technique, called *stress probing*, was first proposed by Bardet in 1989 and is now being considered with growing interest by several authors, in particular for the assessment of the basic features of granular elastoplasticity. In this work, those features were studied in a wide range of material properties (in particular the contact stiffness) and for different deformation regimes (either driven by contact deformation or by network rearrangement). By this method, the validity of the partition hypothesis for the deformation response into separate elastic- and plastic contributions can be clearly assessed; under biaxial loading conditions, the plastic incremental response obeys closely a standard non-associated flow rule with well defined plastic flow direction and yield criterion. A key point for an effective application of the method was clearly the proper choice of the range of stress increments amplitudes for the stress probes, depending on the inherent material properties and deformation regimes.

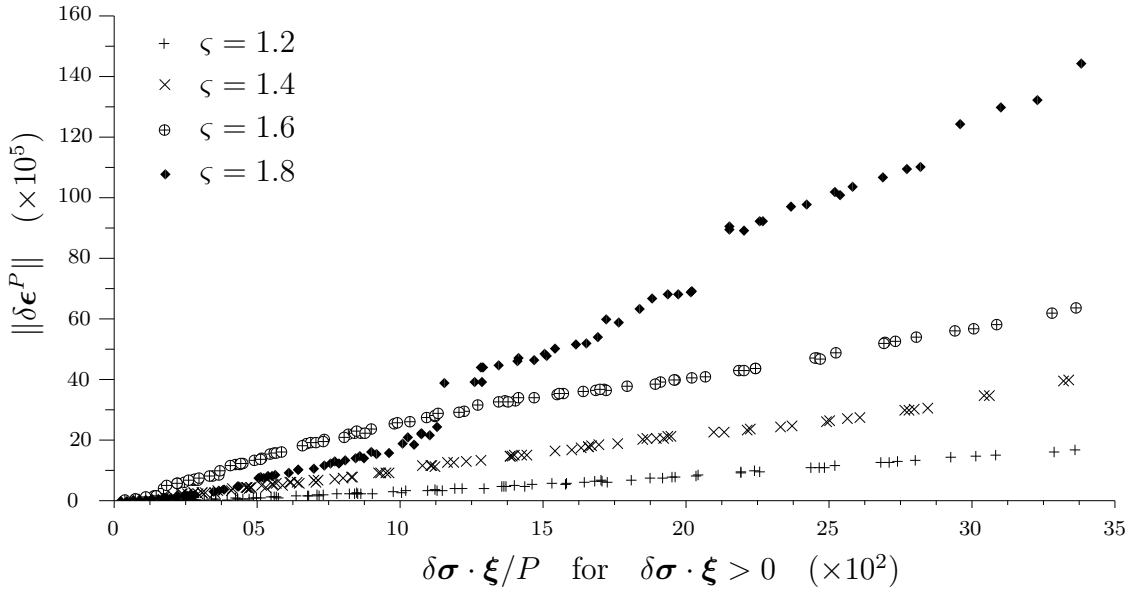


Figure 8: Plastic strain increment amplitude *vs.* active part of the stress increments for specimens at stress ratios $\varsigma \simeq 1.2$ to 1.8 from a biaxial test of family B4. Stress increment amplitudes from $2\sqrt{2}\,P \times 10^{-3}$ to $12 \times 2\sqrt{2}\,P \times 10^{-3}$.

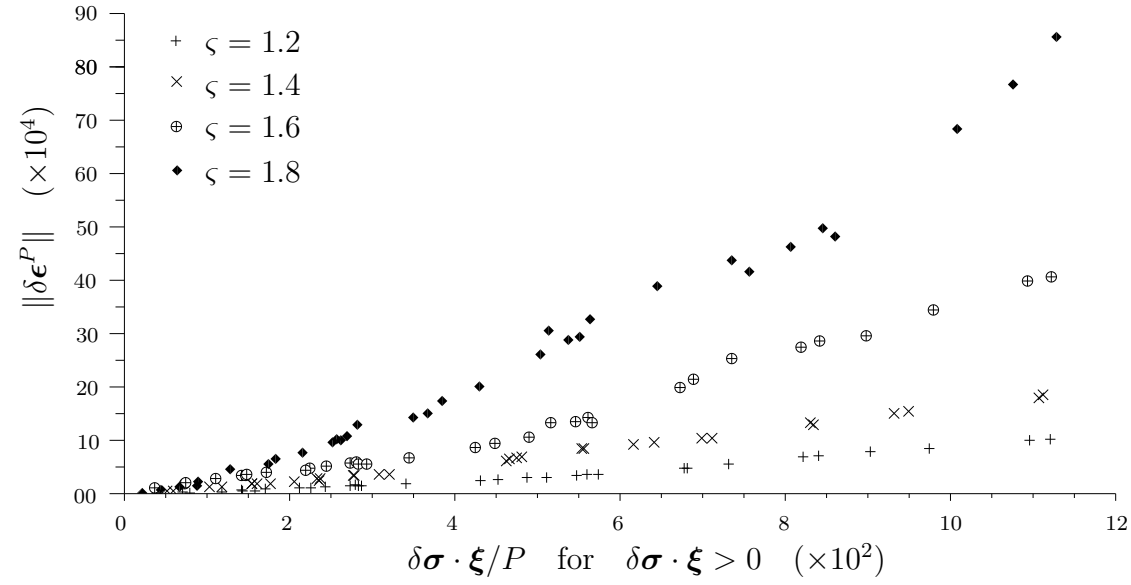


Figure 9: Plastic strain increment amplitude *vs.* active part of the stress increments for specimens at stress ratios $\varsigma \simeq 1.2$ to 1.8 from a biaxial test of family B4. Stress increment amplitudes from $2\sqrt{2}\,P \times 10^{-2}$ to $4 \times 2\sqrt{2}\,P \times 10^{-2}$.

## REFERENCES


[1] Prager, W. and Drucker, D. C. Soil mechanics and plastic analysis for limit design. *Q. Appl. Mathematics* (1952) **2**:157–165.

[2] Schohield, A. N. and Wroth, C. P. *Critical state soil Mechanics*. McGraw-Hill (1968).

[3] Alonso-Marroquín, F. and Herrmann, H. J. Calculation of the incremental stress-strain relation of a polygonal packing. *Phys. Rev. E* (2002) **66**:021301.

[4] Tamagnini, C., Calvetti, F. and Viggiani, G. An assessment of plasticity theories for modelling the incrementally non-linear behavior of granular soils. *J. Eng. Math.* (2005) **52**:265–291.

[5] Darve, F., Sibille, l., Daouadji, A. and Nicot, F. Bifurcations in granular media: macro- and micro-mechanics approaches. *C. R. Mécanique* (2007) **335**:496–515.

[6] Bardet, J. P. and Proubet, J. Applications of micromechanics to incrementally non-linear constitutive equations for granular media. J. In: *Powders and Grains 1989*, J. Biarez, and R. Gourvès, Balkema (ed.), (1989) 265–273.

[7] Bardet, J. P., A Micromechanical Investigation of Incremental Constitutive Equations for Granular Materials. *Int. J. of Plasticity*, (1994) **10**:879–908.

[8] Royis, P. and Doanh, T. Theoretical analysis of strain response envelopes using incrementally non-linear constitutive equations. *Int. Journ. Num. Anal. Meth.* (1998) **22**:97–132.

[9] Froiio, F. and Roux J.-N. Incremental response of a model granular material by stress probing with DEM simulations. In: *IUTAM-ISIMM Symposium on mathematical modeling and physical instances of granular*, AIP Conference Proceedings (2009).

[10] Allen. M and Tildesley D., *Computer simulations of liquids*, Oxford University Press (1987).

[11] Peyneau, P.-E. and Roux, J.-N. Frictionless bead packs have macroscopic friction, but no dilatancy. *Phys. Rev. E*, (2008) **78**:011307.

[12] Roux J.-N. and Combe G. Quasistatic rheology and the origins of strain *C. R. Phys.*, (2002) **3**:131–40.

[13] Agnolin I. and Roux J.-N. Internal states of model isotropic granular packings. I. Assembling process, geometry and contact networks. *Phys. Rev. E* (2007) **76**:061302.

[14] Agnolin I., and Roux J.-N. Internal states of model isotropic granular packings. III. Elastic properties. *Phys. Rev. E*, (2007) **76**:061304.